

1 **A deep learning algorithm using CT images to screen for Corona Virus**

2 **Disease (COVID-19)**

3 Shuai Wang<sup>1,\*</sup>, Bo Kang<sup>2,3,\*</sup>, Jinlu Ma<sup>4,\*</sup>, Xianjun Zeng<sup>5,\*</sup>, Mingming Xiao<sup>1,\*</sup>, Jia

4 Guo<sup>3</sup>, Mengjiao Cai<sup>4</sup>, Jingyi Yang<sup>4</sup>, Yaodong Li<sup>6</sup>, Xiangfei Meng<sup>2,#</sup>, Bo Xu<sup>1,#</sup>

5

6 <sup>1</sup> Department of Molecular Radiation Oncology, National Clinical Research Center  
7 for Cancer, Key Laboratory of Cancer Prevention and Therapy, Key Laboratory of  
8 Breast Cancer Prevention and Therapy, Ministry of Education, Tianjin Clinical  
9 Research Center for Cancer, Tianjin Medical University Cancer Institute and  
10 Hospital, Tianjin 300060, China

11 <sup>2</sup> College of Intelligence and Computing, Tianjin University, Tianjin 300350, China

12 <sup>3</sup> National Supercomputer Center in Tianjin, Tianjin 300457, China

13 <sup>4</sup> Department of Radiation Oncology, First Affiliated Hospital, Xi'an Jiaotong  
14 University, Xi'an, China

15 <sup>5</sup> Department of Radiology, Nanchang University First Hospital, Nanchang, China

16 <sup>6</sup> Department of Radiology, No.8 Hospital, Xi'an Medical College, Xi'an, China

17 \* Equal contribution

18 # Corresponding authors:

19 Bo Xu, MD, PhD

20 Tianjin Medical University Cancer Institute and Hospital

21 Tianjin 300060, China

22 Email: [xubo@tmu.edu.cn](mailto:xubo@tmu.edu.cn)

23

24 Xiangfei Meng, PhD

25 National Supercomputer Center in Tianjin

26 Tianjin 300457, China

27 Email: [mengxf@nscc-tj.cn](mailto:mengxf@nscc-tj.cn)

28

NOTE: This preprint reports new research that has not been certified by peer review and should not be used to guide clinical practice.

29

## Abstract

30

31

32

33

34

35

36

37

38

39

40

**Background:** The outbreak of Severe Acute Respiratory Syndrome Coronavirus 2 (SARS-COV-2) has caused more than 2.5 million cases of Corona Virus Disease (COVID-19) in the world so far, with that number continuing to grow. To control the spread of the disease, screening large numbers of suspected cases for appropriate quarantine and treatment is a priority. Pathogenic laboratory testing is the gold standard but is time-consuming with significant false negative results. Therefore, alternative diagnostic methods are urgently needed to combat the disease. Based on COVID-19 radiographical changes in CT images, we hypothesized that Artificial Intelligence's deep learning methods might be able to extract COVID-19's specific graphical features and provide a clinical diagnosis ahead of the pathogenic test, thus saving critical time for disease control.

41

42

43

44

45

46

47

48

49

**Methods and Findings:** We collected 1,065 CT images of pathogen-confirmed COVID-19 cases (325 images) along with those previously diagnosed with typical viral pneumonia (740 images). We modified the Inception transfer-learning model to establish the algorithm, followed by internal and external validation. The internal validation achieved a total accuracy of 89.5% with specificity of 0.88 and sensitivity of 0.87. The external testing dataset showed a total accuracy of 79.3% with specificity of 0.83 and sensitivity of 0.67. In addition, in 54 COVID-19 images that first two nucleic acid test results were negative, 46 were predicted as COVID-19 positive by the algorithm, with the accuracy of 85.2%.

50

51

**Conclusion:** These results demonstrate the proof-of-principle for using artificial intelligence to extract radiological features for timely and accurate

52 COVID-19 diagnosis.

53 **Author summary**

54 To control the spread of the COVID-19, screening large numbers of suspected  
55 cases for appropriate quarantine and treatment measures is a priority. Pathogenic  
56 laboratory testing is the gold standard but is time-consuming with significant false  
57 negative results. Therefore, alternative diagnostic methods are urgently needed to  
58 combat the disease. We hypothesized that Artificial Intelligence's deep learning  
59 methods might be able to extract COVID-19's specific graphical features and  
60 provide a clinical diagnosis ahead of the pathogenic test, thus saving critical time.  
61 We collected 1,065 CT images of pathogen-confirmed COVID-19 cases along with  
62 those previously diagnosed with typical viral pneumonia. We modified the Inception  
63 transfer-learning model to establish the algorithm. The internal validation achieved  
64 a total accuracy of 89.5% with specificity of 0.88 and sensitivity of 0.87. The  
65 external testing dataset showed a total accuracy of 79.3% with specificity of 0.83  
66 and sensitivity of 0.67. In addition, in 54 COVID-19 images that first two nucleic  
67 acid test results were negative, 46 were predicted as COVID-19 positive by the  
68 algorithm, with the accuracy of 85.2%. Our study represents the first study to apply  
69 artificial intelligence to CT images for effectively screening for COVID-19.

70 **Keywords:** COVID-19, Computed Tomography, Artificial Intelligence, Deep  
71 Learning, Diagnosis

72

## Introduction

73       The outbreak of atypical and person-to-person transmissible pneumonia  
74       caused by the severe acute respiratory syndrome coronavirus 2 (SARS-COV-2,  
75       also known as 2019-nCov) has caused a global alarm. There have been more  
76       than 2.5 million confirmed cases of the Corona Virus Disease (COVID-19) in  
77       the world, as of April 23, 2020. About 16-21% of people with the virus in China  
78       have become severely ill with a 2-3% mortality rate. With the most recent  
79       estimated viral reproduction number ( $R_0$ ), the average number of other people  
80       that an infected individual will transmit the virus to in a completely non-immune  
81       population, stands at about 3.77 [1], indicating that a rapid spread of the  
82       disease is imminent. It is crucial to identify infected individuals as early as  
83       possible for quarantine and treatment procedures.

84       The diagnosis of COVID-19 relies on the following criteria: clinical  
85       symptoms, epidemiological history and positive CT images, as well as positive  
86       pathogenic testing. The clinical characteristics of COVID-19 include respiratory  
87       symptoms, fever, cough, dyspnea, and pneumonia [3-6]. However, these  
88       symptoms are nonspecific, as there are isolated cases where, for example, in  
89       an asymptomatic infected family a chest CT scan revealed pneumonia and the  
90       pathogenic test for the virus came back positive. Once someone is identified  
91       as a PUI (person under investigation), lower respiratory specimens, such as  
92       bronchoalveolar lavage, tracheal aspirate or sputum, will be collected for  
93       pathogenic testing. This laboratory technology is based on real-time RT-PCR

94 and sequencing of nucleic acid from the virus [7,8]. Since the beginning of the  
95 outbreak, the efficiency of nucleic acid testing has been dependent on several  
96 rate-limiting factors, including availability and quantity of the testing kits in the  
97 affected area. More importantly, the quality, stability and reproducibility of the  
98 detection kits are questionable. The impact of methodology, disease stages,  
99 specimen collection methods, nucleic acid extraction methods, and the  
100 amplification system are all determinant factors for the accuracy of test results.  
101 Conservative estimates of the detection rate of nucleic acid are low (between  
102 30-50%) [7,8,9], and tests need to be repeated several times in many cases  
103 before they can be confirmed.

104 Radiological imaging is also a major diagnostic tool for COVID-19. The  
105 majority of COVID-19 cases have similar features on CT images including  
106 ground-glass opacities in the early stage and pulmonary consolidation in the  
107 late stage. There is also sometimes a rounded morphology and a peripheral  
108 lung distribution [6,10]. Although typical CT images may help early screening  
109 of suspected cases, the images of various viral pneumonias are similar and  
110 they overlap with other infectious and inflammatory lung diseases. Therefore, it  
111 is difficult for radiologists to distinguish COVID-19 from other viral pneumonias.

112 Artificial Intelligence involving medical imaging deep-learning systems has  
113 been developed in image feature extraction, including shape and spatial  
114 relation features. Specifically, Convolutional Neural Network (CNN) has been  
115 proven in feature extraction and learning. CNN was used to enhance low-light

116 images from high-speed video endoscopy with the limited training data being  
117 just 55 videos [11]. Also, CNN has been applied to identify the nature of  
118 pulmonary nodules via CT images, the diagnosis of pediatric pneumonia via  
119 chest X-ray images, automated precising and labeling of polyps during  
120 colonoscopic videos, cystoscopic image recognition extraction from videos  
121 [12-15].

122 There are a number of features for identifying viral pathogens on the basis  
123 of imaging patterns, which are associated with their specific pathogenesis [16].  
124 The hallmarks of COVID-19 are bilateral distribution of patchy shadows and  
125 ground glass opacity in early stages. As the disease progresses, multiple  
126 ground glass and infiltrates in both lungs will appear [3]. These features are  
127 quite similar to typical viral pneumonia with only slight differences, which are  
128 difficult to be distinguished by radiologists. Based on this, we believed that  
129 CNN might help us identify unique features that might be difficult for visual  
130 recognition.

131 Hence, the purpose of our study was to evaluate the diagnostic performance of  
132 a deep learning algorithm using CT images to screen for COVID-19 during the  
133 influenza season. To test this notion, we retrospectively enrolled 1,065 CT  
134 images of pathogen-confirmed COVID-19 cases along with previously  
135 diagnosed typical viral pneumonia. Our results reported below demonstrate  
136 the proof-of-principle using the deep learning method to extract radiological  
137 graphical features for COVID-19 diagnosis.

138

## Methods and Materials

139

### Retrospective collection of datasets.

140

We retrospectively collected CT images from 259 patients, in which the

141

cohort includes 180 cases of typical viral pneumonia and the other 79 cases

142

from three hospitals with confirmed nucleic acid testing of SARS-COV-2. In

143

addition, we enrolled additional 15 COVID cases, in which first two nucleic acid

144

tests were negative at initial diagnoses. Hospitals providing the images were

145

Xi'an Jiaotong University First Affiliated Hospital (Center 1), Nanchang

146

University First Hospital (Center 2) and Xi'an No.8 Hospital of Xi'an Medical

147

College (Center 3). All CT images were de-identified before sending for

148

analysis. This study is in compliance with the Institutional Review Board of

149

each participating institutes. Informed consent was exempted by the IRB

150

because of the retrospective nature of this study.

151

### Delineation of ROIs

152

To establish a binary model for distinguishing COVID-19 and typical

153

pneumonia, we drew the Region of Interest (ROI) as input images for the

154

training cohort and validation cohorts. We sketched the ROI from CT images

155

based on features of COVID-19, such as small patchy shadows and interstitial

156

changes in the early stage, multiple ground glass and infiltrates in both lungs in

157

the progression stage, and delineated the ROIs on the CT images of other

158

typical viral pneumonia such as pseudocavity, enlarged lymphnodes and

159

multifocal GGO as the control. The ROIs were divided into three cohorts: one

160

training cohort (n=320 from Center 1), one internal validation cohort (n=455

161 from Center 1) and one external validation cohort (n=290 from Center 2 and 3).

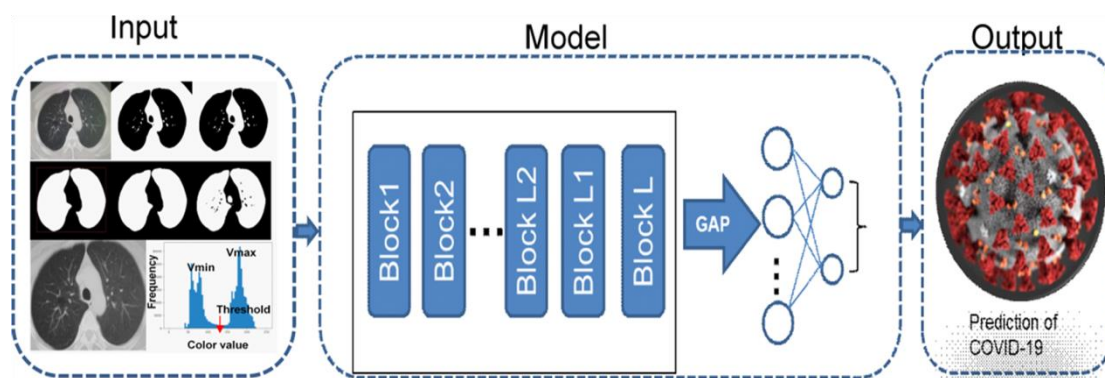
162 For a ROI, it is sized approximately from 395\*223 to 636\*533 pixels.

### 163 **Overview of the proposed architecture**

164 Our systematic pipeline for the prediction architecture is depicted in **Fig 1**.

165 The architecture consists of three main processes: 1) Pre-processing of input  
166 images; 2) Feature extraction of ROI images and training; and 3) Classification  
167 with fully connected network and prediction of multiple classifiers. We built a  
168 transfer learning neural network based on the Inception network. The entire  
169 neural network can be roughly divided into two parts: the first part used a  
170 pre-trained inception network to convert image data into one-dimensional  
171 feature vectors, and the second part used a fully connected network and the  
172 main role is for classification prediction. ROI images from each case were  
173 preprocessed and inputted into the model for training. The number of various  
174 types of pictures in the training set is equal, with a total number of 320. The  
175 remaining CT pictures of each case were used for internal validation. The  
176 model training was iterated 15,000 times with a step size of 0.01.

177



179 **Fig 1.** ROI images extraction and Deep Learning (DL) algorithm framework.



180 ROI images were extracted by the CV model and then trained using a modified  
181 Inception network to extract features. The full connection layer then makes a  
182 classification and prediction.

### 183 **Image preprocessing and feature extraction**

184 Based on the signs of characteristic of pneumonia, ROI images were  
185 defined inflammatory lesions and extracted by our computer vision (CV) model  
186 following the steps. 1) Convert the image to grayscale. 2) Binarize grayscale.  
187 Because using the OSTU's method directly may cause the threshold selection  
188 failure in the case of multi-peaks, the selection of the binarization threshold in  
189 this paper was based on the statistics of all pixel frequency histograms of the  
190 gray color values  $V_{min}$  (80) and  $V_{max}$  (200). The minimum frequency in the  
191 selection interval is threshold, and the interval of frequency statistics is five. 3)  
192 Background area filling. Using the flood filling method to expand the image by  
193 1 black pixel, and fill the black pixels near the border with white. 4) Reverse  
194 color, find all the contour areas of the image, and keep the two largest contour  
195 areas as the two lung areas. 5) Take the smallest bounding rectangle of the  
196 lung area as the ROI frame and crop the original image to obtain the ROI  
197 images. The delineated ROIs were obtained for classification model building.  
198 We modified the typical Inception network, and fine-tuned the modified  
199 Inception (M-Inception) model with pre-trained weights. During the training  
200 phase, the original Inception part was not trained, and we only trained the  
201 modified part. The architecture of M-Inception is shown in **Table 1**. The

202 difference between Inception and M-Inception in classification lies in the last  
 203 fully-connected layers. We reduced the dimension of features before it was  
 204 sent to the final classification layer. The training dataset made up of all those  
 205 patches aforementioned. The Inception network is shown in **Table 1**.

206 **Table 1. The architecture of M-Inception**

|                   | Layer       | Patch size/stride or remarks                 |
|-------------------|-------------|--|
| Inception<br>part | conv        | 3×3/2  |
|                   | conv        | 3×3/1  |
|                   | conv padded | 3×3/1  |
|                   | pool        | 3×3/2  |
|                   | conv        | 3×3/1  |
|                   | conv        | 3×3/2  |
|                   | conv        | 3×3/1  |
|                   | Inception   | 3x, 5x, 2x                                   |
|                   | pool        | 8x8  |
|                   | linear      | logits                                       |
|                   | softmax     | classifier                                   |
| Modified<br>part  | Fc1         | [ batchnorm<br>dropout(0.5)<br>512d Linear ] |
|                   | Fc2         | [ batchnorm<br>dropout(0.5)<br>2d Linear ]   |

207

208 **Prediction.**

209 After generating the features, the final step was to classify the pneumonia  
210 based on those features. Ensembling of classifiers was used to improve the  
211 classification accuracy. In this study, we adopted end-to-end learning to make  
212 the model convergence.

### 213 **Performance evaluation metrics.**

214 We compared the classification performance using Accuracy, Sensitivity,  
215 Specificity, Area Under Curve (AUC), Positive predictive value (PPV), Negative  
216 predictive value (NPV), F1 score and Youden Index. TP and TN represent the  
217 number of true positive or true negative samples. FP and FN mean the number  
218 of false positive or false negative samples. Sensitivity measures the ratio of  
219 positives that are correctly discriminated. Specificity measures the ratio of  
220 negatives that are correctly discriminated. AUC is an index to measure the  
221 performance of the classifier. NPV was used to evaluate the algorithm for  
222 screening, and PPV was the probability of getting a disease when the  
223 diagnostic index is positive. Youden Index was the determining exponent of the  
224 optimal bound. F1 score was a measure of the accuracy of a binary model.  
225 Additionally, performance was evaluated with F-measure (F1) to compare the  
226 similarity and diversity of performance. Kappa value measures the agreement  
227 between the CNN model prediction and the clinical report.

228

229

## Results

230

### Algorithm development.

231

232

233

234

235

236

237

238

239

240

241

242

243

244

245

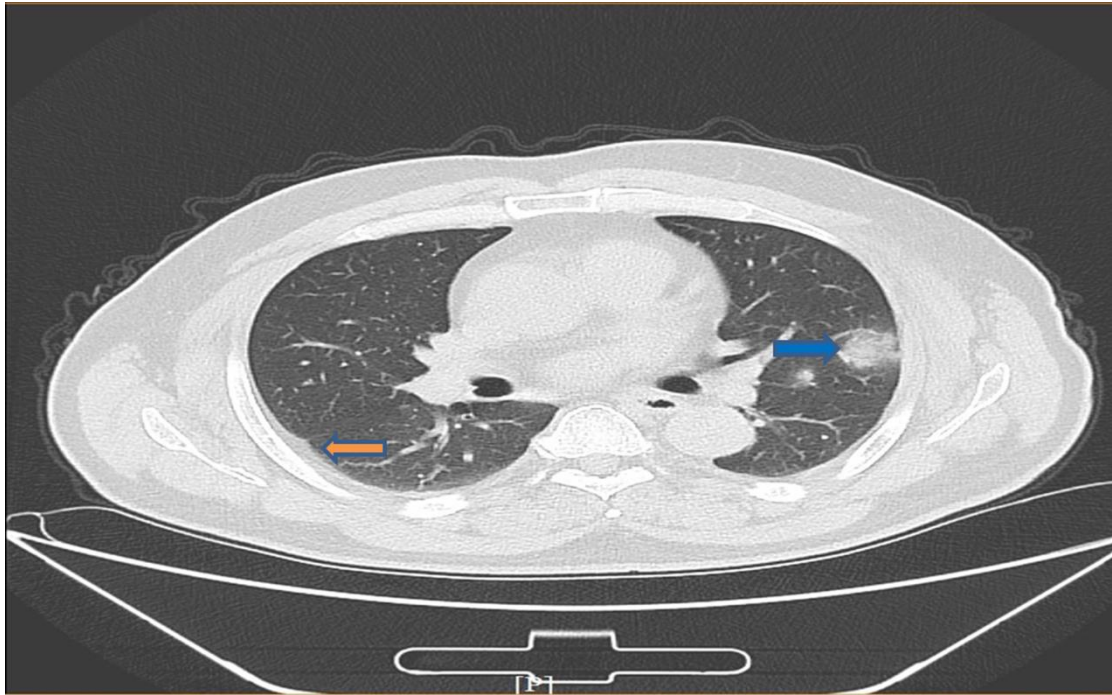
246

247

248

249

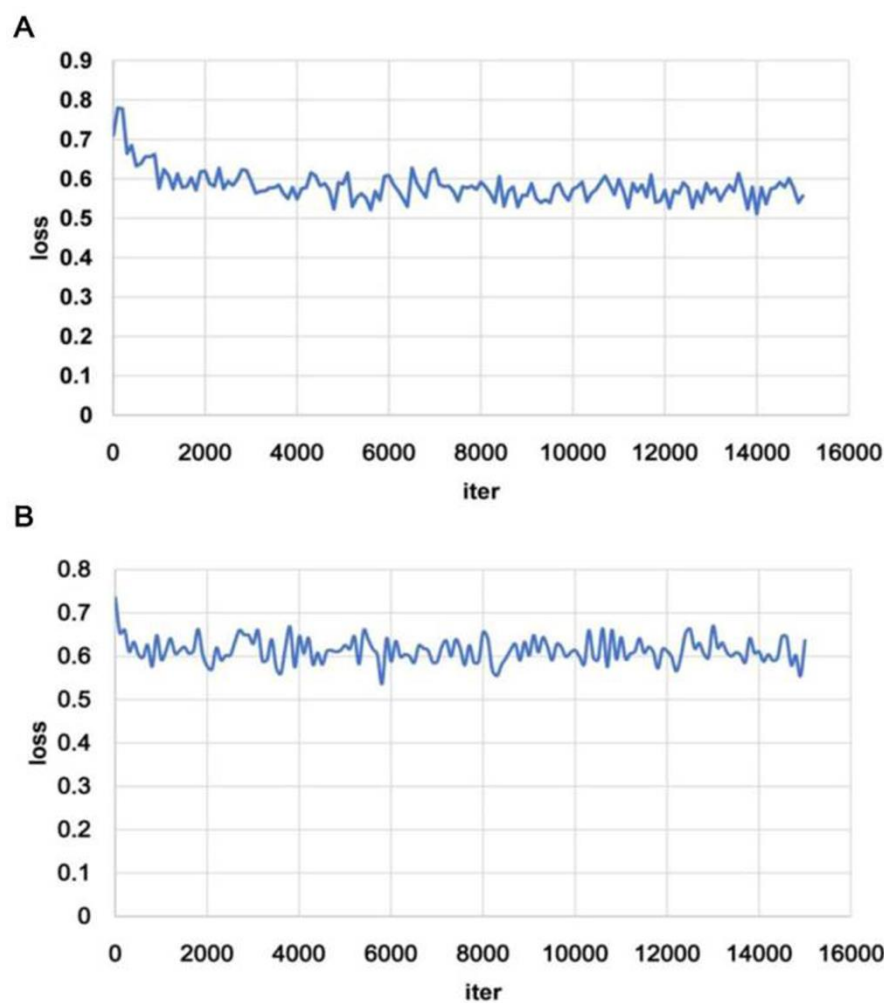
In order to develop a deep learning algorithm for the identification of viral pneumonia images, we initially enrolled 259 patients, in which the cohort includes 180 cases of typical viral pneumonia that were diagnosed previously before the COVID-19 outbreak. These patients are termed COVID-19 negative in the cohort. The other 79 cases were from the three hospitals with confirmed nucleic acid testing of SARS-COV-2, therefore termed COVID-19 positive. Two radiologists were asked to review the images and sketched 1,065 representative images (740 for COVID-19 negative and 325 for COVID-19 positive) for analysis (**Fig 2** is shown as an example). These images were randomly divided into a training set and a validation set. The model training was iterated for 15,000 times with a step size of 0.01. The training loss curve is shown in **Fig 3A**. 320 images (160 images from COVID-19 negative and 160 images from COVID-19 positive) were obtained to construct the model. To test the stability and generalization of the model, 455 images (COVID-19 negative 360 images and COVID-19 positive 95 images) were obtained for internal validation from Center 1 and 290 images (COVID-19 negative 220 images and COVID-19 positive 70 images) were obtained from Center 2 and 3 for external validation. The model training was also iterated for 15,000 times with a step size of 0.01. The training loss curve is shown in **Fig 3B**.



250

251 **Fig 2.** An example of COVID-19 pneumonia features. The blue arrow points to  
252 ground-glass opacity, and the yellow arrow points to the pleural indentation  
253 sign.

254



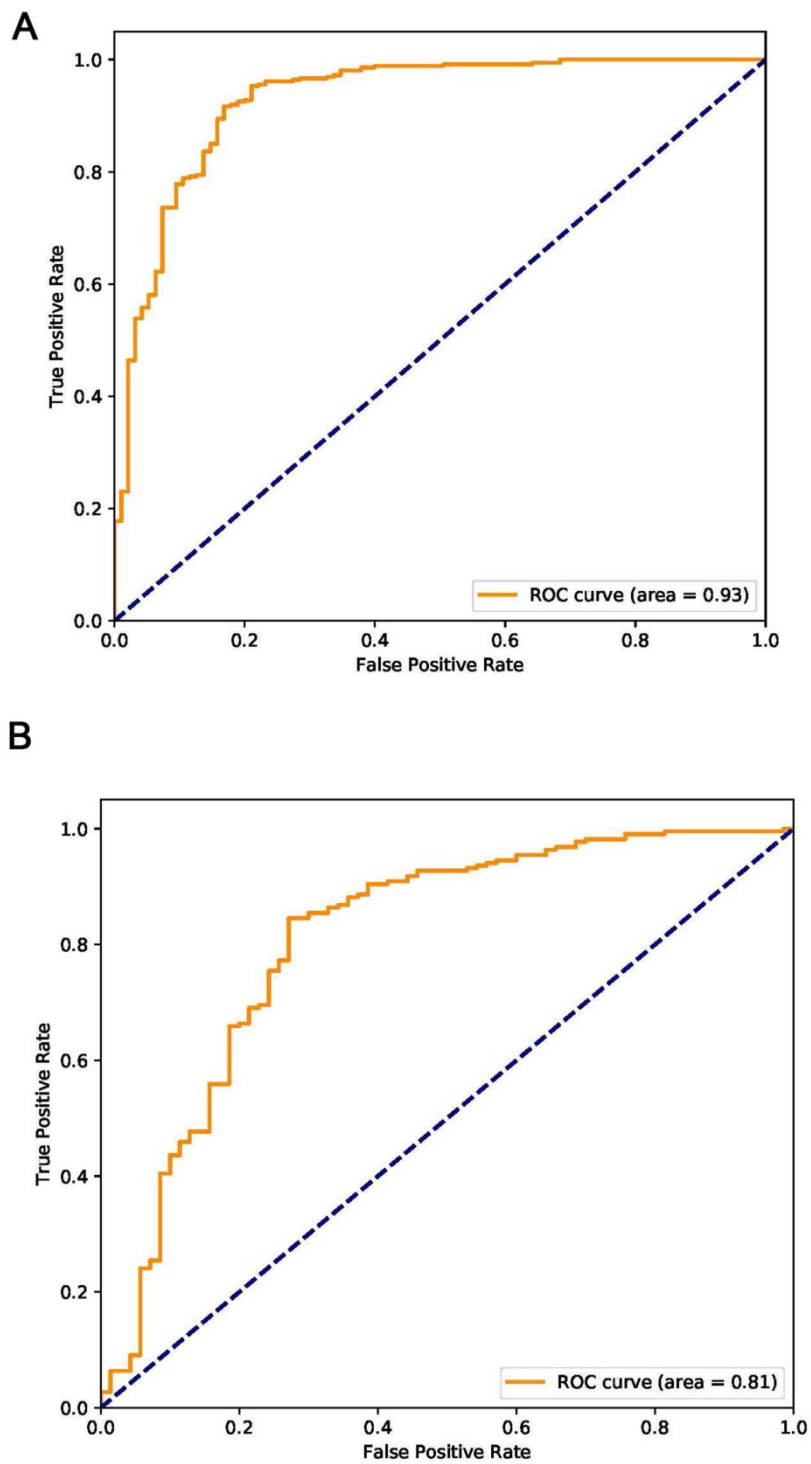
255

256 **Fig 3.** Training loss curves of the models on internal **(A)** and external **(B)**  
257 validation. The loss curve tends to be stable after descending, indicating that  
258 the training process converges

259 **Deep learning performance.**

260 The deep learning algorithm yielded an AUC of 0.93 (95% CI, 0.90 to 0.96)  
261 on the internal validation and 0.81 (95% CI, 0.71 to 0.84) on the external  
262 validation based on the certain CT images **(Fig 4)**. Using the maximized  
263 Youden index threshold probability, the sensitivity was 0.88 and 0.83,

264 specificity 0.87 and 0.67, the accuracy 89.5% and 79.3%, the negative  
265 prediction values 0.95 and 0.90, the Youden indexes 0.75 and 0.48, and the F1  
266 scores were 0.77 and 0.63 for the internal and external datasets, respectively  
267 (**Table 2**). The kappa values were 0.69 and 0.48 for internal and external  
268 validation in certain CT images, indicating that prediction of COVID-19 from  
269 the CNN model is a highly consistent with pathogenic testing results. We also  
270 performed an external validation based on each patient's multiple images. The  
271 accuracy was 82.5%, the sensitivity 0.75, the specificity 0.86, the PPV 0.69,  
272 the NPV 0.89, and the kappa value was 0.59.



273

274 **Fig 4.** Receiver operating characteristic plots for COVID-19 identification for  
275 the deep learning (Inception) algorithm. (A) Internal Validation. (B) External  
276 Validation.

277



278

**Table 2. Deep learning Algorithm Performance**

| Performance Metric | Internal           | External           |
|--------------------|--------------------|--------------------|
| AUC (95%CI)        | 0.93(0.86 to 0.94) | 0.81(0.71 to 0.84) |
| Accuracy, %        | 89.5               | 79.3               |
| Sensitivity        | 0.88               | 0.83               |
| Specificity        | 0.87               | 0.67               |
| PPV                | 0.71               | 0.55               |
| NPV                | 0.95               | 0.90               |
| Kappa*             | 0.69               | 0.48               |
| Yoden index        | 0.75               | 0.50               |
| F1 score‡          | 0.77               | 0.63               |

279 \* Measures the agreement between the CNN model prediction and the clinical

280 diagnosis. ‡Measures the accuracy of the CNN model.

281

### 282 **Comparison of AI with radiologist prediction.**

283 At the same time, we asked two skilled radiologists to assess the 745

284 images for a prediction. Radiologist 1 achieved the accuracy of 55.8% with

285 sensitivity of 0.71 and specificity of 0.51, and Radiologist 2 achieved a similar

286 accuracy of 55.4% with sensitivity of 0.73 and specificity of 0.50 (**Table 3**).

287 These results indicates that it is difficult for radiologists to make prediction of

288 COVID-19 with eye recognition, further showing the advantage of the

289 algorithm we developed.

290

291

292

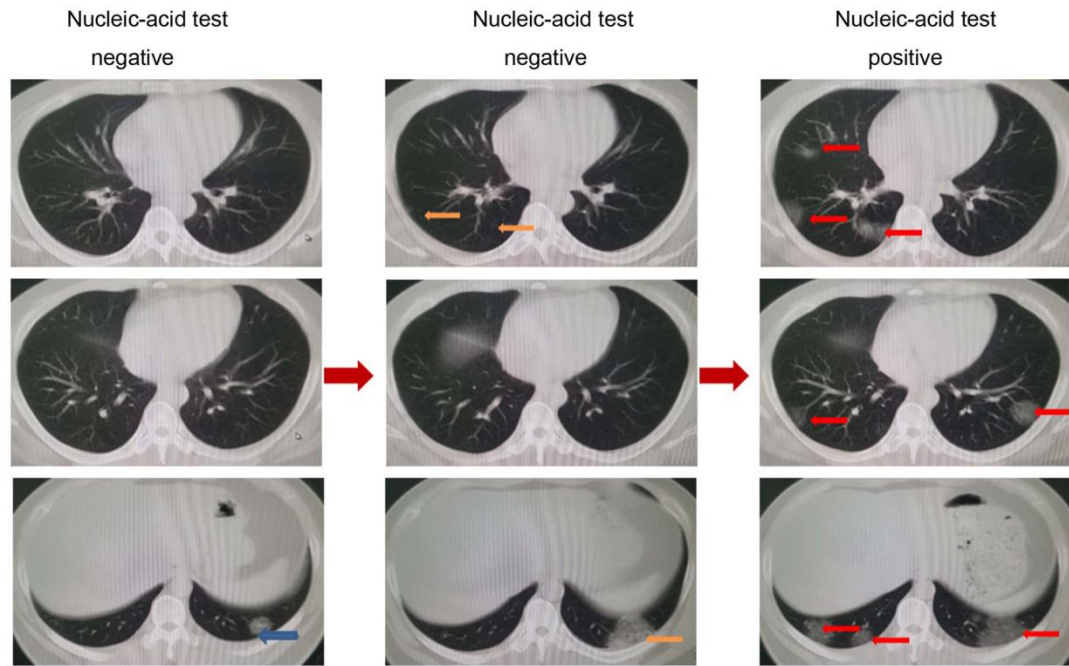
293 **Table 3. Performance metrics for the CNN model versus skilled**  
294 **radiologists.**

| Performance Metric | Internal | External (Based on ROI) | External (Based on patients) | R1   | R2   |
|--------------------|----------|-------------------------|------------------------------|------|------|
| Accuracy, %        | 89.5     | 79.3                    | 82.5                         | 55.8 | 55.4 |
| Sensitivity        | 0.88     | 0.83                    | 0.75                         | 0.71 | 0.73 |
| Specificity        | 0.87     | 0.67                    | 0.86                         | 0.51 | 0.5  |
| PPV                | 0.71     | 0.55                    | 0.69                         | 0.29 | 0.29 |
| NPV                | 0.95     | 0.90                    | 0.89                         | 0.86 | 0.86 |
| F1 score           | 0.77     | 0.63                    | 0.72                         | 0.41 | 0.42 |
| Kappa              | 0.69     | 0.48                    | 0.59                         | 0.15 | 0.15 |
| Yoden index        | 0.75     | 0.50                    | 0.61                         | 0.22 | 0.23 |

295

296 **Prediction of COVID-19 on CT images from pathogenic negative**  
297 **patients.**

298 Because high false negative results were frequently reported from nucleic  
299 acid testing, we aimed to test whether the algorithm could detect COVID-19  
300 when the pathogenic test came negative. To achieve this goal, we enrolled  
301 additional 15 COVID-19 cases, in which initial two nucleic acid tests came  
302 negative and for the third test they became positive. These CT results were  
303 taken on the same day of the nucleic acid tests (**Fig 5**). Interestingly, we found  
304 that, 46 out of the 54 images when nucleic acid test results were negative were  
305 predicted as COVID-19 positive by the algorithm, with the accuracy of 85.2%.  
306 These results indicate that the algorithm has high value serving as a screening  
307 method for COVID-19.



308

309 **Fig 5.** Representative images from a COVID-19 patient with two negatively  
310 reported nucleic acid tests at earlier stages and one final positively reported  
311 test at a later stage. On the left, only one inflammatory lesion (blue arrow) can  
312 be seen near diaphragm. In the middle, lesions (yellow arrows) were found in  
313 two levels of images. On the right, the images were taken on the ninth day  
314 after admission. The inflammation continued to progress, extending to both  
315 lungs (red arrows), and the nucleic acid test became positive.

316

317

## Discussion

318 Timely diagnosis and triaging of PUIs are crucial for the control of  
319 emerging infectious diseases such as the current COVID-19. Due to the  
320 limitation of nucleic acid -based laboratory testing, there is an urgent need to  
321 look for fast alternative methods that can be used by front-line health care  
322 personals for quickly and accurately diagnosing the disease. In the present  
323 study, we have developed an AI program by analyzing representative CT  
324 images using a deep learning method. This is a retrospective, multicohort,  
325 diagnostic study using our modified Inception migration neuro network, which  
326 has achieved an overall 89.5% accuracy. Moreover, the high performance of  
327 the deep learning model we developed in this study was tested using external  
328 samples with 79.3% accuracy. More importantly, as a screening method, our  
329 model achieved a relative high sensitivity, 0.88 and 0.83 on internal and  
330 external certain CT images datasets, respectively. Furthermore, the model  
331 achieved a better profomance on a certain people, the accuracy up to 82.5%.  
332 Of note, our model was used to distinguish between COVID-19 and other  
333 typical viral penumonia, both of which have quite similar radiologic  
334 characteristics. During current COVID-19 global pandemics, the CNN model  
335 can potentially serve as a powerful tool for COVID-19 screening.

336 It is important to note that our model aims to distinguish between  
337 COVID-19 and other typical viral pneumonia, both of which have similar  
338 radiologic characteristics. We compared the performance of our model with

339 that of two skilled radiologists, and our model has shown much higher  
340 accuracy and sensitivity. These findings have demonstrated the  
341 proof-of-principle that deep learning can extract CT image features of  
342 COVID-19 for diagnostic purposes. Using the supercomputer system, the time  
343 for each case takes only about 10 seconds, and it can be performed remotely  
344 via a shared public platform. Therefore, further developing this system can  
345 significantly shorten the diagnosis time for disease control. Our study  
346 represents the first study to apply artificial intelligence technologies to CT  
347 images for effectively screening for COVID-19.

348 The gold standard for COVID-19 diagnosis has been nucleic acid based  
349 detection for the existence of specific sequences of the SARS-COV-2 gene.  
350 While we still value the importance of nucleic acid detection in the diagnosis of  
351 SARS-COV-2 infection, we must also note that the high number of false  
352 negatives due to several factors such as methodological disadvantages,  
353 disease stages, and methods for specimen collection might delay diagnosis  
354 and disease control. Recent data have suggested that the accuracy of nucleic  
355 acid testing is only about 30-50% [6,7,8]. Using CT imaging feature extraction,  
356 we are able to achieve above 89.5% accuracy, significantly outplaying nucleic  
357 acid testing. More interestingly, testing CT images from COVID-19 patients  
358 when initial pathogenic testing came negative, our model has achieved the  
359 accuracy of 85.2% for correctly predicting COVID-19. According to a study  
360 authored by Xia L et al, 75% patients with negative RT-PCR results had

361 positive CT findings [17]. The study recommended that chest CT as a primary  
362 tool for the current COVID-19 detection in epidemic areas.

363 Deep learning methods have been used to solve data-rich biology and  
364 medicine. A large number of labeled data is required for training [18]. Although  
365 we are satisfied with the initial results, we believe that with more CT images  
366 included in the training, we will achieve higher accuracy. Therefore, further  
367 optimizing and testing this system is warranted. To achieve this, we have  
368 generated a webpage that licensed healthcare personnel can access to upload  
369 CT images for testing and validation. The webpage information is as following:  
370 [https://ai.nscg-tj.cn/thai/deploy/public/pneumonia\\_ct](https://ai.nscg-tj.cn/thai/deploy/public/pneumonia_ct).

371 There are some limitations to our study. Although DL has been used to  
372 represent and learn predictable relationships in many diverse forms of data,  
373 and it holds promise for applications in precision medicine, many factors such  
374 as low signal to noise and complex data integration have challenged the DL  
375 efficacy [19]. CT images represent a difficult classification task due to the  
376 relatively large number of variable objects, specifically the imaged areas  
377 outside the lungs that are irrelevant to the diagnosis of pneumonia [12]. In  
378 addition, the training data set is relatively small. The performance of this  
379 system is expected to increase when the training volume is increased. It  
380 should also be noted that, the features of the CT images we analyzed were  
381 from patients with severe lung lesions at later stages of disease development.  
382 Although we have enrolled 15 cases of COVID patients for assessing the value

383 of the algorithm for early diagnosis, larger numbers of database to associate  
384 this with the disease progress and all pathologic stages of COVID-19 is  
385 necessary to optimize the diagnostic system.

386 In future, we intend to link hierarchical features of CT images to features of  
387 other factors such as genetic, epidemiological and clinical information for  
388 multi-modeling analysis for an enhanced diagnosis. The artificial intelligence  
389 system developed in our study should significantly contribute to COVID-19  
390 disease control by reducing the number of PUIs for timely quarantine and  
391 treatment.

392

393 **Ethics Committee Approval and Patient Consent:** This study complies with  
394 the Institutional Review Board of each participating institutes. Informed  
395 consent was exempted by the IRB because of the retrospective nature of this  
396 study.

397 **Funding Source:** None

398 **Competing interests:** The authors have declared that no competing interest  
399 exists

400 **Abbreviations:**

401 COVID-19, Corona Virus Disease

402 CT, Computed Tomography

403 SARS-COV-2, severe acute respiratory syndrome coronavirus 2Convolutional

404 CNN, Neural Network

405 ROI, region of interest

406 M-Inception, modified Inception

407 AUC, Area Under Curve

408 PPV, Positive predictive value

409 NPV, Negative predictive value

410 CV, computer vision

411

412



413

## Reference

- 414 1. Zhou F, Yu T, Du R, Fan G, Liu Y, Liu Z, et al. Clinical course and risk factors  
415 for mortality of adult inpatients with COVID-19 in Wuhan, China: a  
416 retrospective cohort study. *Lancet*. Mar. 2020.
- 417 2. Velavan T, Meyer C. The COVID-19 epidemic. *Trop Med Int Health*, Mar  
418 2020.
- 419 3. Wang D, Hu B, Hu C, Zhu F, Liu X, Zhang J, et al. Clinical Characteristics of  
420 138 Hospitalized Patients With 2019 Novel Coronavirus-Infected Pneumonia  
421 in Wuhan, China. *JAMA*. 2020
- 422 4. Chen N, Zhou M, Dong X, Qu J, Gong F, Han Y, et al. Epidemiological and  
423 clinical characteristics of 99 cases of 2019 novel coronavirus pneumonia in  
424 Wuhan, China: a descriptive study. *Lancet*. 2020.
- 425 5. Li Q, Guan X, Wu P, Wang X, Zhou L, Tong Y, et al. Early Transmission  
426 Dynamics in Wuhan, China, of Novel Coronavirus-Infected Pneumonia. *N Engl*  
427 *J Med*. Mar. 2020.
- 428 6. Huang C, Wang Y, Li X, Ren L, Zhao J, Hu Y, et al. Clinical features of  
429 patients infected with 2019 novel coronavirus in Wuhan, China. *Lancet*. 2020.
- 430 7. Corman VM, Landt O, Kaiser M, Molenkamp R, Meijer A, Chu DK, et al.  
431 Detection of 2019 novel coronavirus (2019-nCoV) by real-time RT-PCR. *Euro*  
432 *surveillance* vol. 25, Jan. 2020.
- 433 8. Chu DKW, Pan Y, Cheng SMS, Hui KPY, Krishnan P, Liu Y, et al. Molecular  
434 Diagnosis of a Novel Coronavirus (2019-nCoV) Causing an Outbreak of

- 435 Pneumonia. *Clinical chemistry*. 2020.
- 436 9. Zhang N, Wang L, Deng X, Liang R, Su M, He C, et al. Recent advances in  
437 the detection of respiratory virus infection in humans. *J Med Virol*. 2020.
- 438 10. Chung M, Bernheim A, Mei X, Zhang N, Huang M, Zeng X, et al. CT  
439 Imaging Features of 2019 Novel Coronavirus (2019-nCoV). *Radiology*. Apr.  
440 2020.
- 441 11. Gomez P, Semmler M, Schutzenberger A, Bohr C, Dollinger M. Low-light  
442 image enhancement of high-speed endoscopic videos using a convolutional  
443 neural network. *Med Biol Eng Comput*. 2019; 57(7): 1451-63.
- 444 12. Choe J, Lee SM, Do KH, Lee G, Lee JG, Lee SM, et al. Deep  
445 Learning-based Image Conversion of CT Reconstruction Kernels Improves  
446 Radiomics Reproducibility for Pulmonary Nodules or Masses. *Radiology*. 2019;  
447 292(2): 365-73.
- 448 13. Kermany DS, Goldbaum M, Cai W, Valentim CCS, Liang H, Baxter SL, et al.  
449 Identifying Medical Diagnoses and Treatable Diseases by Image-Based Deep  
450 Learning. *Cell* 2018; 172(5): 1122-31.
- 451 14. Negassi M, Suarez-Ibarrola R, Hein S, Miernik A, Reiterer A. Application of  
452 artificial neural networks for automated analysis of cystoscopic images: a  
453 review of the current status and future prospects. *World J Urol*. 2020.
- 454 15. Wang P, Xiao X, Glissen Brown JR, Berzin TM, Tu M, Xiong F, et al.  
455 Development and validation of a deep-learning algorithm for the detection of  
456 polyps during colonoscopy. *Nat Biomed Eng*. 2018; 2(10): 741-8.

- 457 16. Koo HJ, Lim S, Choe J, Choi SH, Sung H, Do KH. Radiographic and CT  
458 Features of Viral Pneumonia. *Radiographics*. 2018; 38(3): 719-39.
- 459 17. Ai T, Yang Z, Hou H, Zhan C, Chen C, Lv W, et al. Correlation of Chest CT  
460 and RT-PCR Testing in Coronavirus Disease 2019 (COVID-19) in China: A  
461 Report of 1014 Cases [published online ahead of print, 2020 Feb 26].  
462 *Radiology*. 2020; p.200642.
- 463 18. Ching T, Himmelstein DS, Beaulieu-Jones BK, Kalinin AA, Do BT, Way GP, et  
464 al. Opportunities and obstacles for deep learning in biology and medicine. *J R  
465 Soc Interface*. 2018;15(141):20170387. doi:10.1098/rsif.2017.0387
- 466 19. Grapov D, Fahrman J, Wanichthanarak K, Khoomrung S. Rise of Deep  
467 Learning for Genomic, Proteomic, and Metabolomic Data Integration in  
468 Precision Medicine. *OMICS*. 2018;22(10):630–636.
- 469